Journal of King Saud University – Engineering Sciences (2018) **30**, 286–295

King Saud University

Journal of King Saud University – Engineering Sciences

www.ksu.edu.sa
www.sciencedirect.com

ORIGINAL ARTICLE

A kinetic analysis of the melting HA/Y-PSZ/HDPE nano bio composite for hard tissue materials

Jenan S. Kashan [a,*], Animesh Jha [b], Amin D. Thamir [a], Jafar T. Al-Haidary [a]

[a] *Department of Production Engineering and Metallurgy, University of Technology, Tel Muhammed, Baghdad, Iraq*
[b] *The Institute for Materials Research, Clarendon Road, University of Leeds, Leeds LS2 9JT, UK*

Received 23 May 2015; accepted 24 February 2016
Available online 3 March 2016

KEYWORDS

Biocomposite;
Nano filler;
Melting kinetics;
Crystallisation;
DSC (differential scanning calorimetry).

Abstract Melting characteristics of high-density polyethylene (HDPE) mixed with nano-size ceramic fillers (hydroxyl apatite and yttria stabilised zirconia) was analysed using the isochronal heating rate between 10 °C min^{-1} and 80 °C min^{-1}. In this investigation, the kinetics of melting of HDPE-ceramic composites was analysed using the Avrami equation and the Kissinger model, applied to the Avrami formalism. The magnitude of the apparent energy barrier for the melting of HDPE falls within a range of 12 kJ mol^{-1} and 22 kJ mol^{-1}, with a tendency for heterogeneous melting which was determined by characterising the value of Avrami exponent, *n* found to vary between 1 and 2. The heterogeneous nature of melting was also confirmed using the scanning electron microscopy, from which the evidences for both nano- and micro-scale interactions of HDPE with ceramic fillers (HA and yttria stabilised zirconia) were confirmed on a microscopic scale.

1. Introduction

Hydroxyapatite (HA: $Ca_{10}(PO_4)_6(OH)_2$) is one of the main constituents of bones and is the only inorganic part of mammalian bone structure. At present there is an urgent need for using the grafts for replacing damaged bone, which might be achieved via any of either endogenous or exogenous materials: auto graft, allograft or a xenograft. Both auto grafts and allografts are proving difficult to access for medical reasons and due to the shortage of supply, which is why the popular alternative is to have a xenograft, which must be biocompatible. For xenografts, hydroxyapatite HA is widely used for research (Wang, 2003) and in commercial products, however this mineral is intrinsically weak and has to be used with another load-bearing material for making a structure which is comparable with natural bone (Wang et al., 1998).

Amongst a range of implant and bone analogue materials, since 80 s, the HA reinforced with high-density polyethylene (HDPE) is the commercial brand (HAPEX™), which has been quite well proven for its biocompatibility (Yari Sadi et al., 2006). This is because the HA mimics natural bone, and when processed with micro- and macro porous scaffolds, the osteoinduction commences well by absorbing bone morphogenic proteins, growth factors, and progenitor stem cells.

Abbreviations: HA, hydroxyapatite; Y-PSZ, yttria partial stabilised zirconia.

* Corresponding author. Mobile: +964 7703816971.
E-mail address: jsk_jsk2012@yahoo.com (J.S. Kashan).

Peer review under responsibility of King Saud University.

ELSEVIER Production and hosting by Elsevier

http://dx.doi.org/10.1016/j.jksues.2016.02.005

Once osteoconduction commences in the composite structure, the process of osseointegration takes over locally by allowing the formation of collagen (Weiner and Wagner, 1998).

Bone, as a composite, has a complex microstructural feature which has been a major challenge in mimicking its load-bearing performance, when designing with HA based composite. In order to overcome the poor strength and elastic modulus of HA, the polymer-based bio-composite as materials engineering approach has been developed (Evans et al., 1990) for bone graft and suitable implant materials (Tripathi et al., 2010). The review (Tripathi et al., 2010) presents a comparison of mechanical properties including the coefficient of friction and wear rates against ceramic and metal surfaces. The role of HDPE in the artificial bone composite is to provide the intermediate functions of collagen, which is essential for bone function, as it is anisotropic in its load-bearing properties (Bonefield, 2006; Kong et al., 1999; Yari Sadi et al., 2004). The incorporation of HDPE with ceramic fillers therefore provides the much needed mechanical compatibility, which otherwise is difficult to engineer in synthetic composites. Most importantly, HDPE is biocompatible and does not produce any toxins (Evans et al., 1990; Kong et al. 1999; Tripathi et al., 2010) which hinder osteogenesis and osseointegration.

In brief, the literature so far strongly suggests that the interaction of ceramic particulates with HDPE determines the tensile strength and fracture behaviour of the HDPE-HA composites, which has formed the basis for selecting the nano particles of HA and zirconia for bio-composite materials engineering (Huang et al., 2009; Wang and Bonefield, 2001; Zhuang and Aizawa, 2013).

Recently, nano-scale HA (10–100 nm) has received much attention owing to its superior functional properties (Zhu et al., 2004), compared with the micrometre-scale HA materials. The nano-sized HA structure is also known for promoting pre osteoblast adhesion, differentiation and proliferation, and setting up the transport of calcium ions for osteoconduction (Silvio et al., 2002). Relevant osteogenic processes occur in nano-HA structure at a much faster rate than that reported for the micro- and macro-HA (Yari Sadi et al., 2008; Wang and Bonefield, 2001). In HA, the addition of zirconia increases strength and elastic modulus (Bonefield, 2006, Tripathi et al., 2010).

The main aim of this article is to characterise the kinetics of melting of HDPE in the presence of nano-scale HA and Y_2O_3-partial stabilised zirconia (Y-PSZ). Since the HDPE is a low melting (130 °C) material, implying that in the composite structure, the creep flow and viscous properties might be governed by the nano-scale interaction with the high melting point ceramic phases, which we aim to analyse using DSC. To the best of our knowledge, the kinetics of melting of HDPE in the presence of nano-scale (10–100 nm) particulates, especially of HA and zirconia are not reported.

The effect of different types of ceramic fillers on the rheological and thermal properties of polymer matrix were investigated previously (Chafidz et al., 2011; Joseph et al., 2002; Khasraghi et al., 2011), however in this study our focus is on the role of nano sized fillers on the melting kinetics for HDPE composite, as an approach to understanding the nano particulate filler-polymer matrix interaction which is also examined, in light of the potential use of such materials as implant or graft. The viability of osteoblasts are known to be dependent on the materials structure, especially surface properties which in such composites might be dependent on the structural relaxation, e.g. flow behaviour during fabrication. On the melting of HDPE with different ceramic filler phases the literature is limited (Alothman et al., 2014; Chen et al., 2013; Cupta et al., 1994). More specifically no report on the influence of nano-particulates of HA and Y-PSZ with HDPE on thermal behaviour and kinetics of melting are known, correlating with the microstructural changes.

2. Experimental

2.1. Preparation of nano-composite materials

HDPE powder with average particle size of 5 μm and the powder density 0.959 g cm^{-3} was used as a matrix material for the fabrication of bio-composite material for bone grafting.

Two different types of ceramic filler materials were used: (a) 99% pure HA having 20 nm average particle size and a particle density of 3.140 g cm^{-3}, and (b) partially-stabilised zirconia (ZrO_2-PSZ) which was doped with 3 mol% of yttria (Y_2O_3). The Y-PSZ nano powder was 99.9% pure and had an average particle size of 40 nm and density of 5.91 g cm^{-3}. Powders were dry mixed in a ball mill and then hot pressed at 140 °C, using 140 MPa compression pressure, after which the disc shape test samples with 15 mm diameter and height varying between 7 and 10 mm were obtained.

2.2. Differential scanning calorimetric (DSC) measurements

For the characterisation of melting properties of the bio-composites, the Perkin–Elmer DSC-8000 Thermal Analyzer was used.

The sample size for each scan varied in the range of 10–12 mg. Two different scanning conditions were applied: (a) several isochronal rates (10, 15, 20, 25, 30, 35, 40, and 80 °C min^{-1}) of scanning for heating ramp and a fixed cooling rate of 150 °C min^{-1} were adopted. (b) in the second type of scan the rates for heating and cooling were maintained at 5, 10, 20, 30, 40 and 80 °C min^{-1}.

2.3. Determination of kinetics parameters

For determining the kinetics of melting, we adopted the technique used for measuring the rate of devitrification of a glass (Jordan and Jha, 1994; Sandler et al., 2003), which is based on the Kissinger method for the analysis of Avrami model for phase transformation kinetics (Avrami, 1941; Chen, 1978; Kissinger, 1957). The reason for choosing this method is quite apparent due to the similarity in the thermal behaviour during heating and cooling cycle of an HDPE and a glass. In a multicomponent system, the melting rate is dependent on the rate of heating which is why it is essential to use the single-scan differential scanning plots for melting at different rates for the characterisation of rate of melting in the nano-composite ceramic mixed HDPE. As an example, a single scan non-isothermal DSC plot is shown in Fig. 1, from which the onset of melting T_o, peak of melting T_p, and the heat of fusion data are obtained. In this figure, the values of T_o and T_p were calculated from the intersection of the extrapolated linear section of the falling peak edge with the baseline and from the

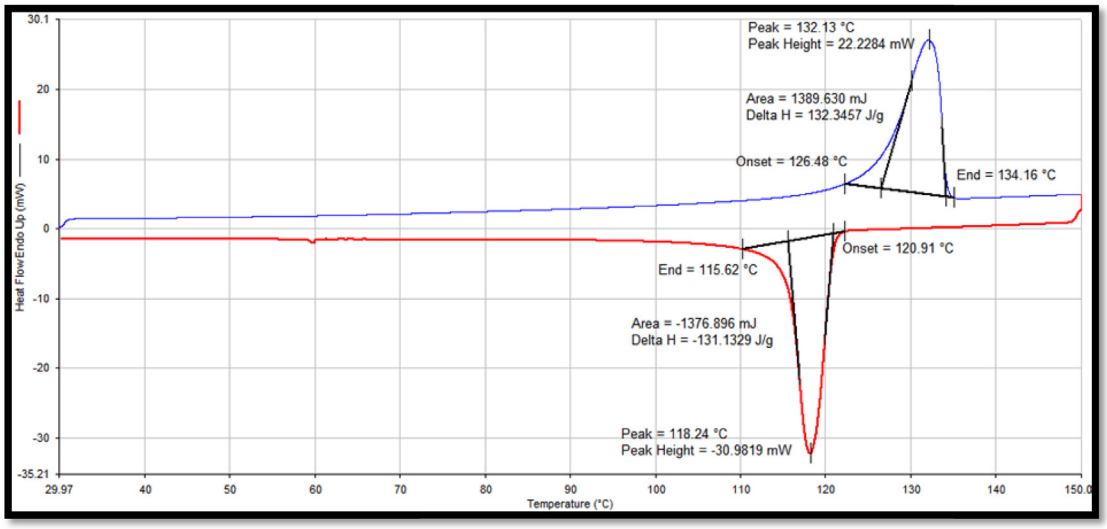

a

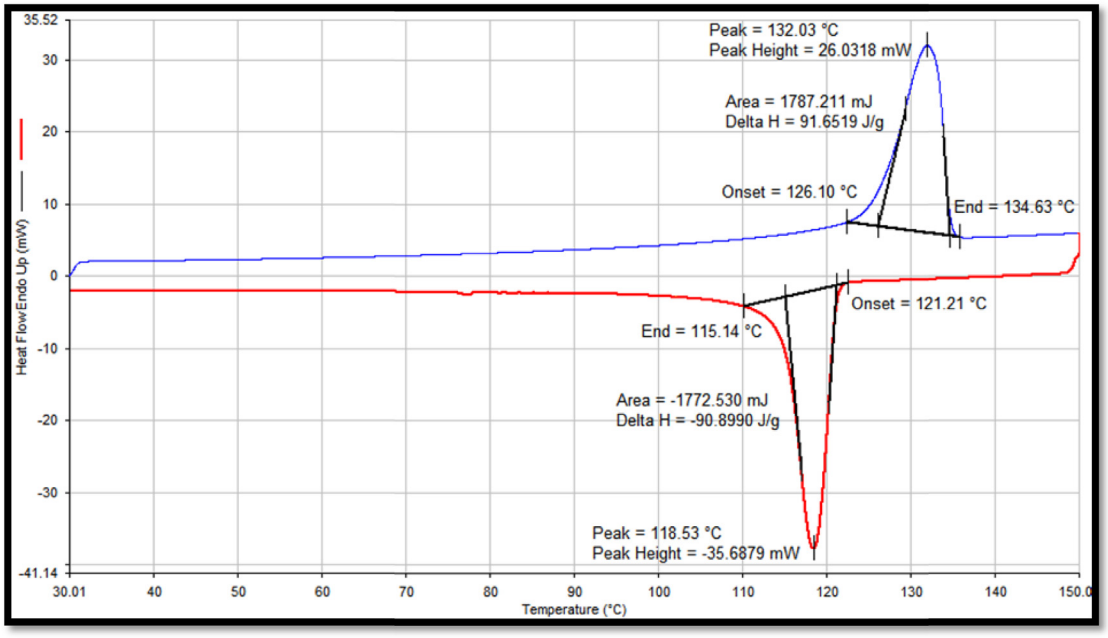

b

Figure 1 Estimated data form DSC scan for (a) 20 vol% HA/HDPE, (b) for 20 vol% HA/20 vol% Y-PSZ/HDPE samples.

maximum point in the endothermic peak, respectively. The heat of fusion (ΔH_m) was determined by integrating the area under the endothermic peak (Jordan and Jha, 1994).

In our method of analysis, the influence of different ceramic phases on the kinetics of melting of HDPE is also examined by recoding the enthalpy changes, associated with the scan rate imposed for each sample. Assuming that the particulate-ceramic filler interaction is chemical (Chrissafisa and Bikiaris, 2011), one might then expect a melting behaviour which might be comparable with the changes in a multicomponent system. In this respect a non-isothermal melting and crystallisation might be attributed to a large number of infinitesimally small isothermal melting and crystallisation events, which might be homogeneously distributed in the specified volume. The variables, therefore associated within the assumptions of Avrami model, are the average for the events under consideration. Using the Avrami model, the volume fraction (X) of the HDPE material melted can be explained by the following equation as a function of time (t):

$$X = 1 - \exp(-kt)^n \quad (1)$$

where k is a rate factor affecting melting, t is the time in seconds and n is an exponent. Since the quantity k is a rate factor, it can be then represented by the standard Arrhenius rate equation, which under non-isothermal scanning condition will be relevant in determining the rate parameter in the specified

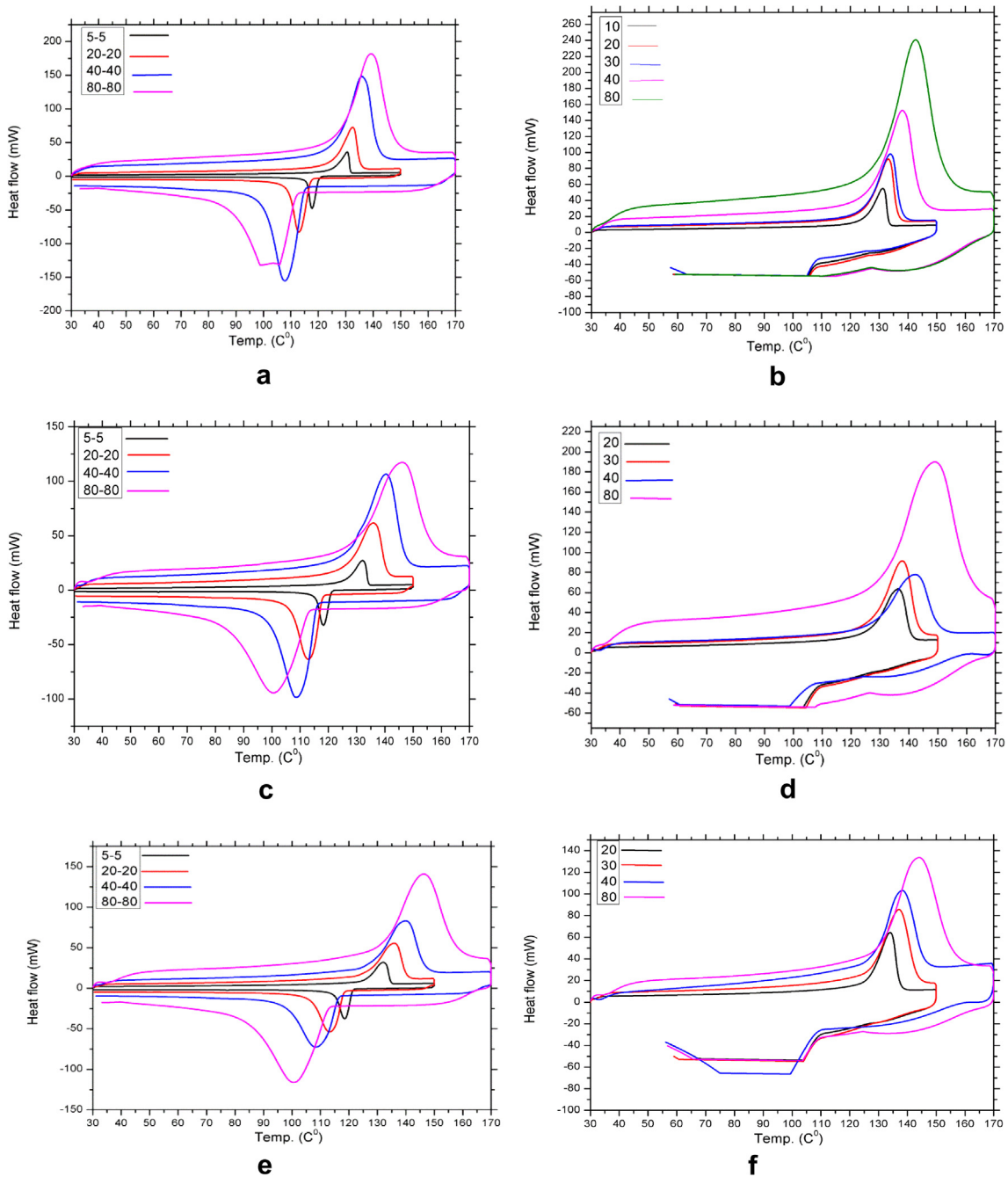

Figure 2 DSC scan (a) HDPE at different heating–cooling rates, (b)HDPE at different cooling rates-constant cooling rate, (c) 20 vol% HA/HDPE at different heating–cooling rates, (d) 20 vol% HA/HDPE at different cooling rates-constant cooling rate, (e) 10 vol% Y-PSZ/20 vol% HA/HDPE at different heating–cooling rates, and (f) 10 vol% Y-PSZ/20 vol% HA/HDPE at different cooling rates-constant cooling rate.

temperature range. Using Eq. (2), the temperature dependence of rate law may be defined for melting reaction in accordance with the Arrhenius law:

$$k = k_o \cdot \exp\left(-\frac{E_m}{RT}\right) \tag{2}$$

where k_o is a frequency factor, E_m is the apparent activation energy, and R is the universal gas constant (8.314 J mol^{-1} K^{-1}). In the realm of Avrami model, the Ozawa-Chen Eq. (3) (Avrami, 1941; Chen, 1978; Kissinger, 1957) may be employed for the characterisation of k_o and E_m by measuring the shifts in the melting temperatures with various heating rates, discussed above:

$$\ln\left(\frac{T_p}{\beta}\right) = \frac{E_m}{RT_p} + \left(\frac{1}{n}\right)\ell n[-\ell n(1-X)] - \ln\left(\frac{k_o}{2}\right) \tag{3}$$

From Eq. (3), a plot of $\ln(T_p/\beta)$ against the reciprocal of T_p, should yield a straight line with gradient equal to E_m/R for each heating–cooling cycle. Each value of slope was used to derive the value of apparent activation energy of melting of

HDPE, mixed with nano-sized ceramic fillers. Once the value of E_m is determined, the value of exponent n was evaluated using relationship, proposed by Piloyan et al. (Piloyan et al., 1966; Zhuang and Aizawa, 2013).

$$\frac{nE_m}{R} = \left(\frac{d\ell n(\Delta y)}{d\left(\frac{1}{T}\right)}\right) \tag{4}$$

where Δy is the displacement of the non-isothermal DSC trace from the base line. Plotting $\ln(\Delta y)$ against $1/T$, yields a straight line with a slope of nE_m/R, from which the value of n may be derived. Since the HDPE is a crystalline polymer which on mixing creates a heterogeneous material, and as a result of mixing with the ceramic fillers whether all of the HDPE undergoes melting is unclear. The degree of melting however may be ascertained by measuring the fractional enthalpy, defined below in Eq. (5) (Joseph et al., 2002). In Eq. (5), the melted fraction (X) in a given composite is defined by the fractional enthalpy (ΔH_m) by taking the ratio of enthalpy per unit mass from a given composite which is then normalised with respect to the enthalpy of 100% HDPE (ΔH_o) per unit mass:

$$X = \left[\frac{\Delta H_m}{\Delta H_o}\right] \tag{5}$$

The mass enthalpy of HDPE characterised by DSC measurements was 290 J g^{-1} and is consistent with the literature data (Piloyan et al., 1966).

2.4. Microstructure analysis

The morphological and microstructural characterisation of HA/HDPE and Y-PSZ/HA/HDPE composite surfaces were examined using a LEO-1530 scanning electron microscopy.

Specific attention was paid for the preparation of non-conducting composite bio-composite samples which were secured onto the specimen holders by conducting carbon cement, then sputter-coated with less than 10 nm thick layer of Pd–Pt alloy film. This approach for sample preparation permitted the imaging of ceramic particulates at high magnification without charging, which is often seen during SEM imaging of non-conducting bone and skeletal minerals.

3. Results and discussion

3.1. Melting and crystallisation behaviour under different isochronal heating rates and fixed and varying cooling rates

For the composite with 20 vol% HA the graphical illustrations are presented in Fig. 2c and d; the trends identified therein are also apparent in other composites which we have investigated and are summarised in Table 1a. The results of apparent peak shifts under varying isochronal heating rate (20–80 °C min^{-1}) conditions are compared in Fig. 2b, d, and f, in which during the cooling cycle of 150 °C min^{-1} there are no discernible peaks

Table 1a Comparison of the peak (T_p) and onset (T_o) temperatures (°C) under two different heating and cooling rate conditions.

Variable heating rates between 10° and 80 °C min^{-1}. Cooling rate = 150 °C min^{-1}					Variable heating and cooling rates between 10° and 80 °C min^{-1}				
Monolithic/composite materials	β	$^{\neq}T_p$	$^{*}T_o$	ΔH_m, J g^{-1}	Monolithic/composite materials	β	$^{\neq}T_p$	$^{*}T_o$	ΔH_m, J g^{-1}
HDPE									
	10	131	125	153		5	153	125	132
	15	132	126	138		10	146	125	133
	20	133	126	202		20	127	126	133
	25	134	126	151		40	121	127	136
	30	134	126	138		80	129	129	139
	35	136	126	155					
	40	138	128	194					
	80	143	131	191					
20 vol% HAp									
	10	134	127	140		5	132	126	132
	15	135	127	143		10	153	126	134
	20	136	127	153		20	166	127	136
	25	137	128	131		40	151	128	140
	30	138	128	165		80	95	131	146
	35	138	128	130					
	40	142	128	138					
	80	149	132	145					
20 vol% HAp + 10 vol% Y-PSZ									
	10	133	126	106		5	92	126	132
	15	134	126	99		10	94	126	134
	20	134	127	92		20	100	127	136
	25	137	128	102		40	87	129	140
	30	137	128	94		80	93	133	146
	35	138	128	95					
	40	138	129	93					
	80	144	132	100					

$^{\neq}$ Melting peak temperature.
* Start melting temperature.

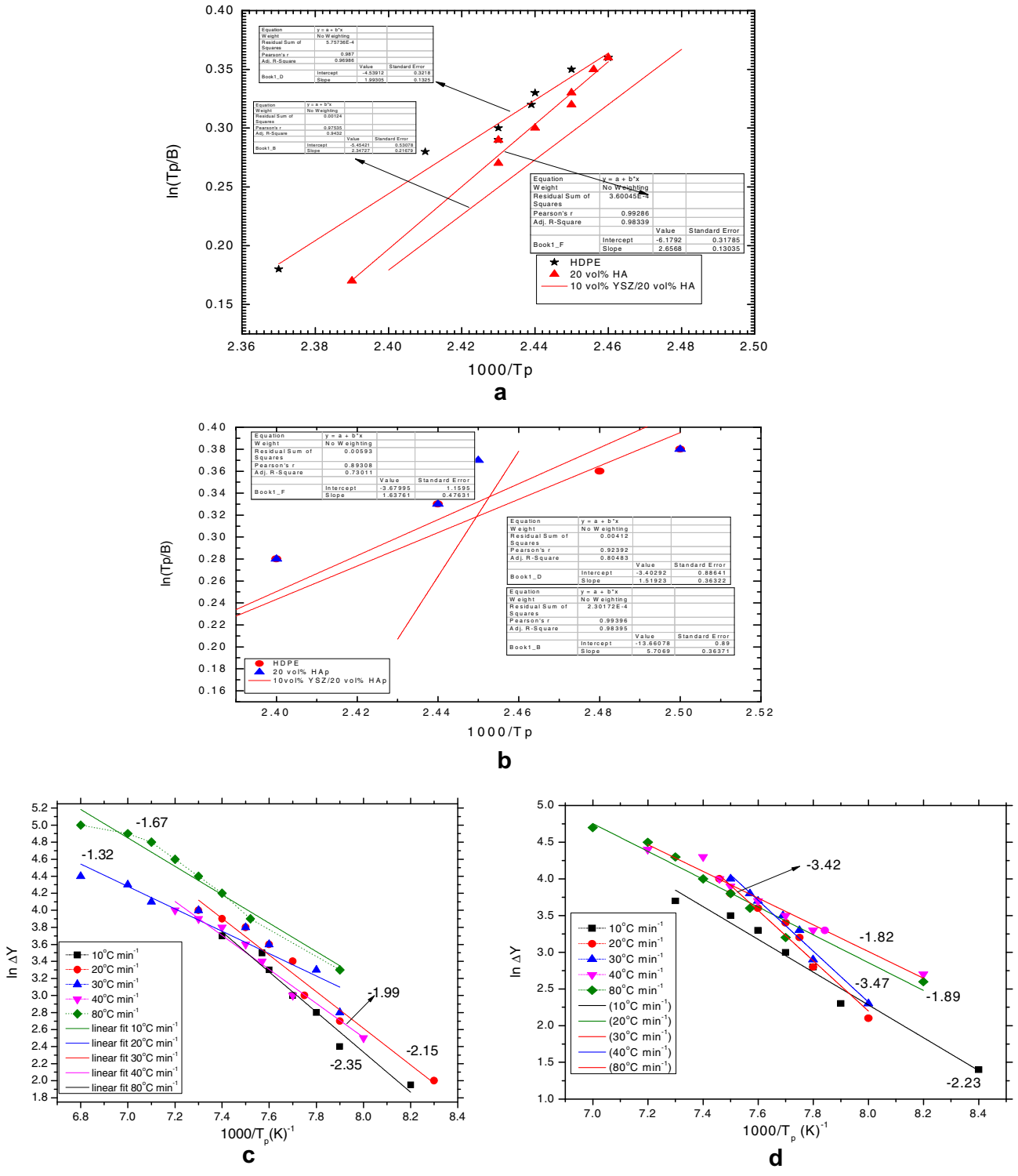

Figure 3 Relationship between $\ln(T_p/\beta)$ vs $1000/T_P$: (a) at different heating rate-constant cooling rate, (b) at different heating–cooling rates, (c) Relationship between $\ln \Delta Y$ vs $1000/T_p$ for 10 vol% YSZ/20 vol% HA/HDPE composite at different heating rate-constant cooling rate, (d) at different heating cooling rate.

of crystallisation. On the other hand, when the heating and cooling rates were identical, both the melting peaks on heating ramp and crystallisation peaks on cooling cycle appear almost in similar shape and symmetry. These melting peaks are spaced apart shifting to higher temperatures with increasing heating rates. The area under melting and crystallisation peaks increase with the increasing ramp rate. By contrast, the crystallisation peaks, which are exothermic in nature, shift to lower temperatures with the increasing area under the crystallisation peaks. The change in the shape and peak position as a function of

Table 1b Derived values of apparent activation energy (E_m, J mol^{-1}) of HDPE and the Avrami exponent, n.

Variable heating rates between 10° and 80 °C min^{-1}. Cooling rate = 150 °C min^{-1}						Variable heating and cooling rates between 10° and 80 °C min^{-1}					
Monolithic/ composite materials	β	×Ec kJ/mol	n^*	$K^{\neq}$	Xc%**	Monolithic/ composite materials	β	×Ec kJ/mol	n^*	$K^{\neq}$	Xc%**
HDPE											
	10	19	0.7	$3.97*10^{-3}$	52		5–5	47	0.74	$1.18^{*}10^{-6}$	39
	15		1.4		47		10–10		0.61		50
	20		0.78		69		20–20		0.52		43
	25		0.87		52		40–40		0.41		41
	30		0.96		47		80–80		0.35		44
	35		0.9		53						
	40		0.77		66						
	80		0.77		65						
20 vol% HAp											
	10	17	1.17	$11*10^{-3}$	48		5–5	8	3.21	0.12	45
	15		1.12		49		10–10		3.01		53
	20		1.07		52		20–20		2.23		57
	25		1.07		45		40–40		1.77		52
	30		0.64		56		80–80		1.66		32
	35		1		44						
	40		0.97		48						
	80		0.78		50						
	10	22	0.84	$2*10^{-3}$	48		5–5	6	4.68	0.27	31
	15		1.1		34		10–10		4.23		32
	20		1.28		31		20–20		3.38		34
	25		0.91		35		40–40		3.18		30
	30		1.31		32		80–80		2.77		32
	35		0.75		32						
	40		0.72		48						
	80		0.71		34						

x: Activation energy.
* Avrami constant.
$^{\neq}$ Constant of reaction.
** Crystallinity%.

heating and cooling rates clearly illustrate that there is a kinetic barrier for both the melting and crystallisation cycles. The characteristic temperatures T_p and T_o with the enthalpy of fusion (J g^{-1}) data are shown in Table 1a, for HDPE, HDPE with 20% HA, and HDPE with 20% HA and 10 vol% Y-PSZ. All DSC scans show a single endothermic peak for melting. In previous research reports (Chafidz et al. 2011; Chen et al., 2013; Piloyan et al., 1966), the existence of the single endo or exothermic peak in a thermal scan has been attributed to the occurrence of co-crystallisation, and these are further analysed by characterising the half-width of a peak. From Table 1a, it is apparent that the onset and peak temperatures vary with the heating rate systematically, in accordance with the theory described above in Eq. (3). However the variation in the area under the peak (enthalpy change) either with the heating rate or the shift in T_p/T_o is unclear. However in this investigation since the ceramic phase does not demonstrate any significant phase transformation during thermal scan, it is largely thermally passive and the only changes apparent are in HDPE.

The values of the apparent activation energy E_m and Avrami exponent n are determined from the linear regression analysis of the plots for the heating and cooling conditions, defined above in Section 2.2. From the data in Table 1a, the linear regression analysis was carried out for each data set in Fig. 3a and b, for deriving the values of apparent activation energy of melting, E_m and the Avrami exponent n, respectively. These data for heating and cooling cycles investigated for HDPE, 20% Y-PSZ HDPE, and 20% HDPE/10% HA/HDPE materials are summarised in Table 1b, from which it is clear that the apparent activation energy E_m varies with ceramic loading from 15 ± 4 kJ mol^{-1} to 47 ± 3 kJ mol^{-1}. Based on these data the values of exponent, n may be determined from the average value of the slopes in Fig. 3b and d. From the analysis, the derived values of n in this investigation fall well below 4; a value which corresponds to the condition for three dimensional continuous and homogeneous melting in the confined volume. The magnitude of heterogeneity increases as n becomes smaller than 4, which is the condition we observe from thermal analysis.

The derived value of activation energy also depicts a range suggesting that the melting kinetics may be dependent on the microscopic and sub-microscopic interactions of HDPE in the presence of Y-PSZ and HA materials. Given the spread of variation in the data, except for HDPE under different heating and cooling rates which yields a value of 47 ± 3.0 kJ mol^{-1}, the values of E_m only vary within a narrow range of ±5 kJ mol^{-1} with an average value of E_m at 17 kJ mol^{-1}.

3.2. Microstructure

The main reason for such a small but discernible change does not become clear until the detailed scanning electron microscopic image analysis of the two types of HDPE composites, which are shown in Figs. 4 and 5. In Fig. 4a–d, the microstructural features of composite with 20 vol% HA are summarised at different magnifications, illustrating the morphological features of nano HA particles and their clustering in Fig. 5a and particle matrix interaction in and resulting changes in the microstructures, Fig. 4b. For example the shear-like band formation in Fig. 4a and b are a clear sign of strong particle matrix interaction, via which the difference in the elastic constants of the two materials (HDPE matrix and HA particulates) lead to the shearing of the HDPE matrix. These shear bands also seem to trap smaller particles of HA in Fig. 4b, which must have folded and flowed under load during composite fabrication. The heating and cooling cycle during thermal analysis does seem to significantly alter these shear band characteristics, which can only be analysed in detail using sub-ambient DSC by monitoring the glass transition temperature close to liquid nitrogen temperature. In our investigation using

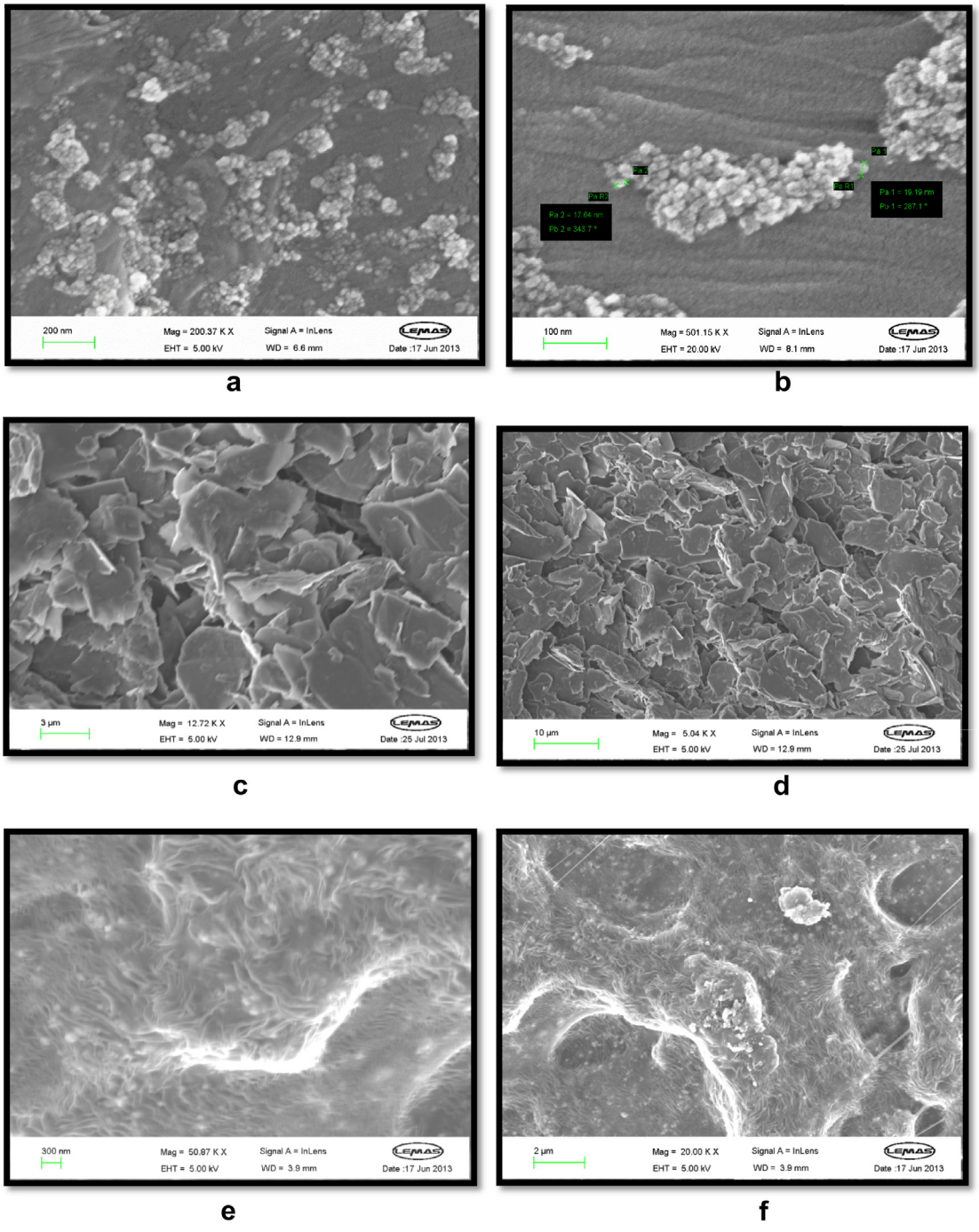

Figure 4 SEM images for (a, b) 20 vol%, HA/HDPE samples, (c–f) 20 vol%, Y-PSZ/20 vol%, HA/HDPE samples.

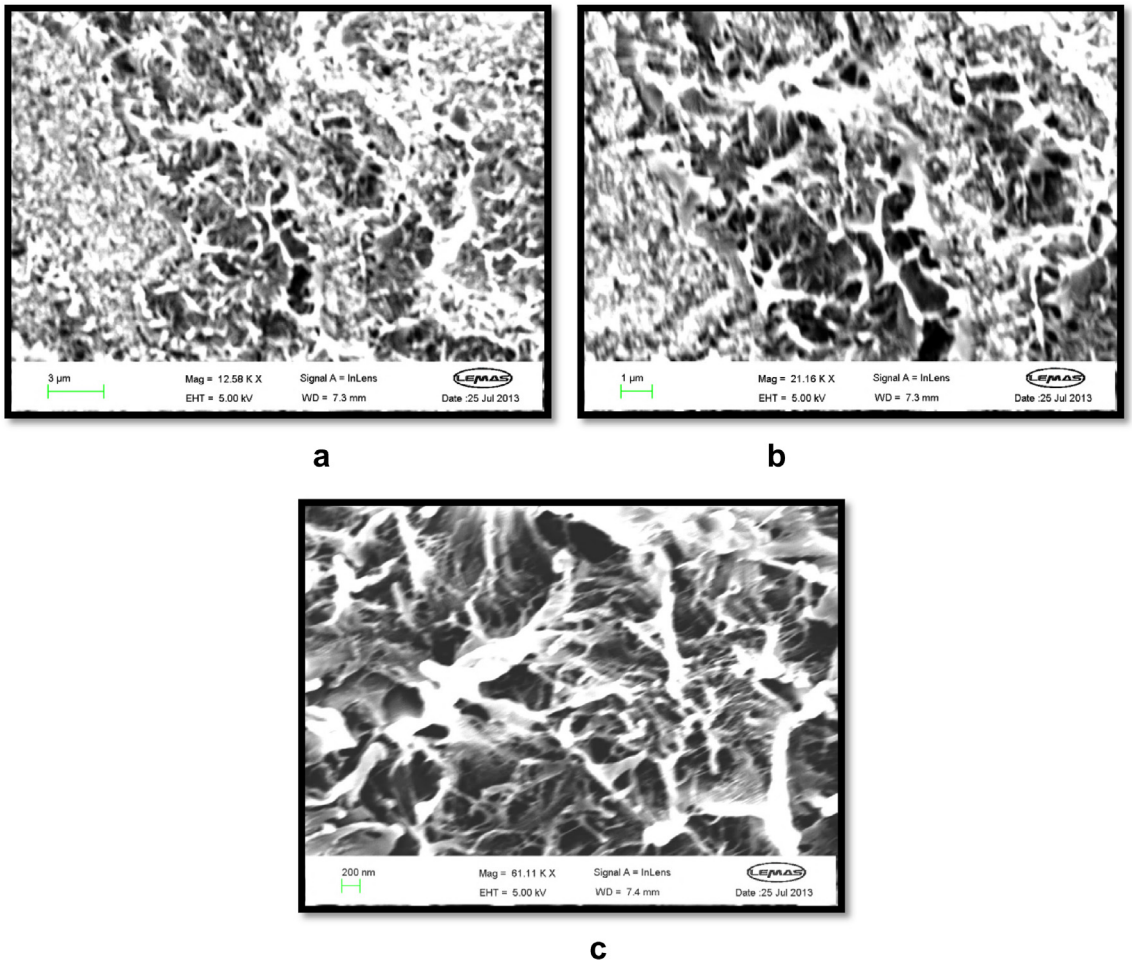

Figure 5 SEM images for 10 vol% Y-PSZ/20 vol% HA composite fracture surface at different magnifications.

DSC we attempted to examine the changes in the glass transition temperatures, however the operational range of DSC (−50 °C below 0 °C) did not reveal any change in the glass transition temperature of HDPE. In Fig. 4b we also see clearly the sites from where the particles might have been released, which suggests that the nano particle trapping and shear band formation are not the only features of particle–matrix interaction in the 20 vol% HA containing HDPE. Clusters of nanometre size particles might be interacting much more differently due to their aggregated size than the individual particles.

In the composite containing 20 vol% Y-PSZ/20 vol% HA, quite different structure has been obtained which is a flake like structure that is similar to bone structure (Fig. 4c, and d). This fibroses structures are very close to the natural bone structure which reflect high mechanical properties as listed in our previous studies (Kashan et al., 2014; Kashan, 2014).

In Fig. 5a–c, the fracture morphological features of 20 vol % HA with HDPE and HDPE with 20 vol% HA with 10 vol% YSZ are shown, from which it is apparent that the microstructural features are very different compared with the 20 vol% HA. The SEM micrographs at high magnifications in these two figures show the particles and associated porosities, shear band features which are much more random in appearance, when compared with the flow-like appearance in Fig. 4a and b. This difference is clearly arising due to the presence of zirconia and perhaps overall higher loading of HDPE matrix with the ceramic phase.

For osteoblast growth such high surfaces are morphological features which are highly desirable, as they mimic the sub-structural features of bone. It is for this reason the melting behaviour and kinetics of melting are relevant, for ensuring that the composite materials maintain the high-surface area for encouraging cell growth, without which such HDPE-based ceramic composites have little use as bone graft materials.

4. Conclusions

The melting kinetics of HDPE dispersed with 20 vol% HA and 20% HA and 10 vol% PSZ nano-scale ceramic powders were characterised using the Kissinger method, described in Eq. (3). The apparent activation energy of melting, which ranged between 15 kJ mol^{-1} and 47 kJ mol^{-1}, was found to be strongly dependent on the volume fraction of ceramic phase present. With the increasing volume fraction of ceramic phase, the derived values of Avrami exponent, n were found to be much smaller than 4 indicating a strong presence of heterogeneous melting. The extent of heterogeneous melting was apparent from the high-magnification SEM images showing the evidences for shear bands, particle clustering, and particle

release. These microstructural evidences allude to indirect evidences for localised phase change, the chemistry of which is unclear.

Acknowledgements

The authors acknowledge Mr M. Javed and Mr John Harrington at the Institute for Materials Research at the University Of Leeds, Leeds in UK for his technical support in the areas of DSC and SEM facilities, respectively.

References

Alothman, Y., Fouad, H., Al-Zahrani, S.M., Ayman, E., Mohammed, F., Ansari, S., 2014. Thermal, creep-recovery and viscoelastic behavior of high density polyethylene/hydroxyapatite nano particles for bone substitutes: effects of gamma radiation. BioMed. Eng. OnLine 13, 1–15.

Avrami, M., 1941. Kinetics of phase change. III. granulation, phase change, and microstructure. Chem. Phys. 9 (2), 177–184.

Bonefield, W., 2006. Hydroxyapatite reinforced polyethylene as an analogues materials for bone replacement. Ann. N.Y. Acad. Sci. 523, 173–177.

Chafidz, Ali, A., Al-haj, M., Elleithy, R., 2011. Morphological, thermal, rheological, and mechanical properties of polypropylene-nanoclay composites prepared from master batch in a twin screw extruder. Mater. Sci. 46, 6075–6086.

Chen, S.H., 1978. A method for evaluating viscosities of metallic glasses from the rates of thermal transformations. Non-Cryst. Solids 27, 257–263.

Chen, X., Shi, J., Wang, L., Shi, H., Liu, Y., 2013. Preparation and Evaluation of Nano-Hydroxyapatite/Poly (Styrene-Divinylbenzene) Porous Microsphere for Aspirin Carrier, Wiley Online Library, Doi: http://dx.doi.org/10.1002/pc.2102.

Chrissafisa, K., Bikiaris, D., 2011. Can nanoparticles really enhance thermal stability of polymers? Part I: an overview on thermal decomposition of addition polymers. Thermochim. Acta 523, 1–24.

Cupta, A.K., Rana, S.K., Deopura, B.L., 1994. Crystallization kinetics of high-density polyethylene/linear low-density polyethylene blend. Appl. Polym. Sci. 51, 231–239.

Evans, G.P., Behiri, J.C., Currey, J.D., Bonfield, W., 1990. Microhardness and Young's modulus in cortical bone exhibiting a wide range of mineral volume fractions, and in a bone analogue. J. Mater. Sci. Mater. Med. 1, 38–43.

Huang, S.B., Gao, S.S., Yu, H.Y., 2009. Effect of nanohydroxyapatite concentration on remineralization of initial enamel lesion in vitro. Biomed. Mater. 4, 1–6.

Jordan, W.G., Jha, A., 1994. A review of the role of DSC analysis in the design of fluorozirconate glasses for fiber optic applications. Therm. Anal. 42, 759–770.

Joseph, R., McGregor, W.J., Martyn, M.T., Tanner, K.E., Coates, P. D., 2002. Effect of hydroxyapatite morphology/surface area on the rheology and processability of hydroxyapatite filled polyethylene composites. Biomater 23, 4295–4302.

Kashan, Jenan S., 2014. Preparation and characterization of hydroxyapatite/yttria partially stabilized zirconia polymeric biocomposite Ph.D. thesis. UOT.

Kashan, Jenan S., Thamir, A.D., Al-Haidary, Jafar T., 2014. Effect of particle size on the physical and mechanical properties of nano HA/HDPE bio-composite for synthetic bone substitute. Eng. Technol. 32 (2), 286–297.

Kissinger, H.E., 1957. Reaction kinetics in differential thermal analysis. Anal. Chem. 29, 1702–1706.

Kong, Y.M., Kim, S., Kim, H.E., 1999. Reinforcement of hydroxyapatite bioceramic by addition of ZrO_2 coated with Al_2O_3. Am. Ceram. Soc. 82 (11), 2963–2968.

Piloyan, G.O., Rybachikov, I.D., Rybachikov, O.S., 1966. Determination of activation energies of chemical reactions by differential thermal analysis. Nature 212, 1229. http://dx.doi.org/10.1038/2121229a0.

Yari Sadi, A., Homaeigohar, S., Khavandi, A., Javadpour, J., 2004. The effect of partially stabilized zirconia on the mechanical properties of the hydroxyapatite–polyethylene composites. J. Mater. Sci. Mater. Med. 8, 853–857.

Sandler, J.K.W, Kirk, J.E., Kinloch, I.A., Shaffer, M.S.P, Windle, A. H., 2003. Ultra-low electrical percolation threshold in carbon-nanotube-epoxy composites. Polymer 44, 5893–5899.

Silvio, L.D., Dalby, M.J., Bonfield, W., 2002. Osteoblast behaviour on HA/PE composite surfaces with different HA volumes. Biomater 23, 101–107.

Khasraghi, S., Rezaei, M., Karim M., Aghjeh, R, 2011. In: Proceedings of the Polymer Processing Society Asia/Australia Regional Meeting – PPS-November 15–17, Kish Island (Iran).

Tripathi, G., Choudhury, P., Basu, B., 2010. Development of polymer based biocomposites: a review. Mater. Tech. 25, 158–176.

Wang, M., 2003. Developing bioactive composite materials for tissue replacement. Biomater 24, 2133–2151.

Wang, M., Bonefield, W., 2001. Chemically coupled hydroxyapatite-polyethylene composites: structure and properties. Biomater 22, 1311–1320.

Wang, M., Joseph, R., Bonfield, W., 1998. Hydroxyapatite-polyethylene composites for bone substitution: effects of ceramic particle size and morphology. Biomater 19, 2357–2366.

Weiner, S., Wagner, H.D., 1998. The Material Bone: structure-mechanical function relations. Ann. Rev. Mater. Sci. 28, 271–298.

Yari Sadi, A., Shokrgozar, M., Homaeigohar, S., Khavandi, A., 2006. The effect of partially stabilized zirconia on the biological properties of HA/HDPE composites in vitro. J. Mater. Sci. Mater. Med. 17, 407–412.

Yari Sadi, A., Shokrgozar, M., Homaeigohar, S., Khavandi, A., 2008. Biological evaluation of partially stabilized zirconia added HA/HDPE composites with osteoblast and fibroblast cell lines. J. Mater. Sci. Mater. Med. 19, 2359–2365.

Zhu, S.H., Huang, B.Y., Zhou, K.C., Huang, S.P., Liu, F., Li, Y., Li, Y.M., Xue, Z.G., Long, Z.G., 2004. Hydroxyapatite nanoparticles as a novel gene carrier. J. Nanopart. Res. 6, 307–311.

Zhuang, Zhi., Aizawa, M., 2013. Protein adsorption on single-crystal hydroxyapatite particles with preferred orientation to a(b)- and c-axes. J. Mater. Sci. Mater. Med. 24, 1211–1216.